ACS APPLIED MATERIALS & INTERFACES
Research Article
www.acsami.org

Interface and Transport Properties of Metallization Contacts to Flat and Wet-Etching Roughed N-Polar n-Type GaN

Liancheng Wang,* Zhiqiang Liu, Enqing Guo, Hua Yang, Xiaoyan Yi,* and Guohong Wang

Semiconductor Lighting Technology Research and Development Center, Institute of Semiconductors, Chinese Academy of Sciences, Beijing 100083, China

Supporting Information

ABSTRACT: The electrical characteristics of metallization contacts to flat (F-sample, without wet-etching roughed) and wet-etching roughed (R-sample) N-polar (Nitrogen−polar) n-GaN have been investigated. R-sample shows higher contact resistance (R_c) to Al/Ti/Au (∼2.5 × 10^{-5} Ω·cm^2) and higher Schottky barriers height (SBH, ∼0.386 eV) to Ni/Au, compared with that of F-sample (∼1.3 × 10^{-6} Ω·cm^2, ∼0.154 eV). Reasons accounting for this discrepancy has been detail investigated and discussed: for R-sample, wet-etching process caused surface state and spontaneous polarization variation will degraded its electrical characteristics. Metal on R-sample shows smoother morphology, however, the effect of metal deposition state on electrical characteristics is negligible. Metallization contact area for both samples has also been further considered. Electrical characteristics of metallization contact to both samples show degradation upon annealing. The VLED chip (1 mm × 1 mm), which was fabricated on the basis of a hybrid scheme, coupling the advantage of F- and R-sample, shows the lowest forward voltage (2.75 V@350 mA) and the highest light output power.

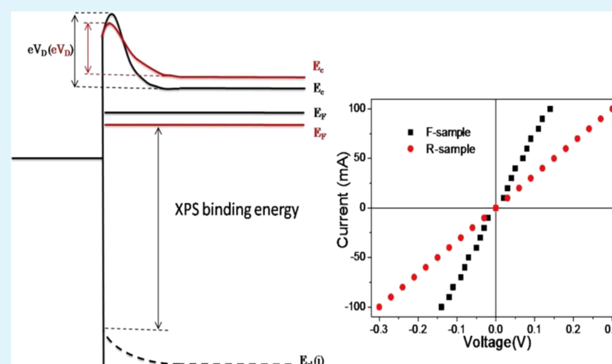

KEYWORDS: *metallization contacts, N -polar, GaN, electrical characteristics, vertical light emitting diodes*

1. INTRODUCTION

Recently, vertical GaN-based light-emitting diodes (VLEDs), which was fabricated via insulating sapphire substrate removal and thermal and electrical conductive substrate transfer, has been investigated extensively. It is considered to be the candidate for future high power and high efficiency LED device thanks to its better electrical, thermal and optical characteristics.[1−3] With the deposited top n-contact and bottom p-contact, VLEDs show vertical current injection geometry. Generally speaking, the n-contact in VLEDs is deposited on N-polar n-GaN, which is different with conventional lateral LEDs (L-LEDs), whose n-contact is deposited on Ga-polar n-GaN. Electrical characteristics of N-polar n-contact have been investigated extensively previously and its thermal instability has been confirmed by many reports.[4,5] It was attributed to the presence of the complex surface states of N-polar GaN, consisting of impurities and process-induced donorlike and acceptorlike defects.

On the other hand, N-polar n-GaN is usually surface roughed by the wet-etching method to improve the extraction efficiency of emitted photos by reducing total internal reflection at the GaN/air interface.[6] Hexagonal and dodecagon pyramids[7] with various sizes will distribute randomly on the surface after wet-etching in KOH or H_3PO_4 etchant. What should be noted is that the n-contact is actually mostly deposited on the sidewalls of the pyramids after the roughening process,[6−8] in contrast to its fully deposition on flat N-polar surface. There should be many differences of n-contact to flat and roughed N-polar n-GaN. However, almost all the articles reported before were based on contacts to flat N-polar n-GaN, and to the best of our knowledge, there was no investigation into the electrical characteristics of the contacts to wet-etching roughed N-polar surface.

In our previous study,[8] we have reported the differences of the contacts deposited on wet-etching roughed and unroughed surface of N-polar GaN; however, there is still a lack of deep investigation of the specific inner mechanism. In this paper, we first present the full comparison study of metallization contacts to flat (F-sample, see the Supporting Information, Figure 1) and wet-etching roughed N-polar n-GaN (R-sample, see the Supporting Information, Figure 1) further in detail. It was found that R-sample exhibits higher R_c to Al/Ti/Au and higher SBH to Ni/Au. XPS measurements were performed to investigate the surface state before and after the surface roughing. Spontaneous polarization and deposited metal states of both samples have also been investigated. Metallization contact area to both samples has also been discussed. The annealing process was also adopted to investigate the thermal stability of both samples. VLEDs chips were finally assembled.

Received: April 13, 2013
Accepted: May 28, 2013
Published: May 28, 2013

© 2013 American Chemical Society

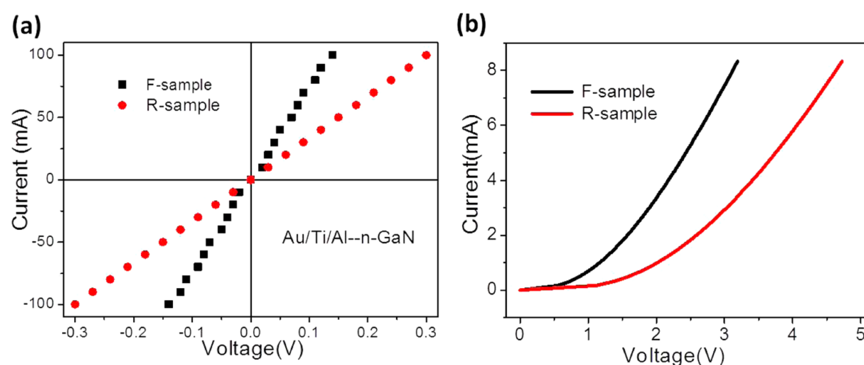

Figure 1. Voltage−current (*I*−*V*) characteristics of (a) Al/Ti/Au and (b) Ni/Au contacts to F-sample and R-sample.

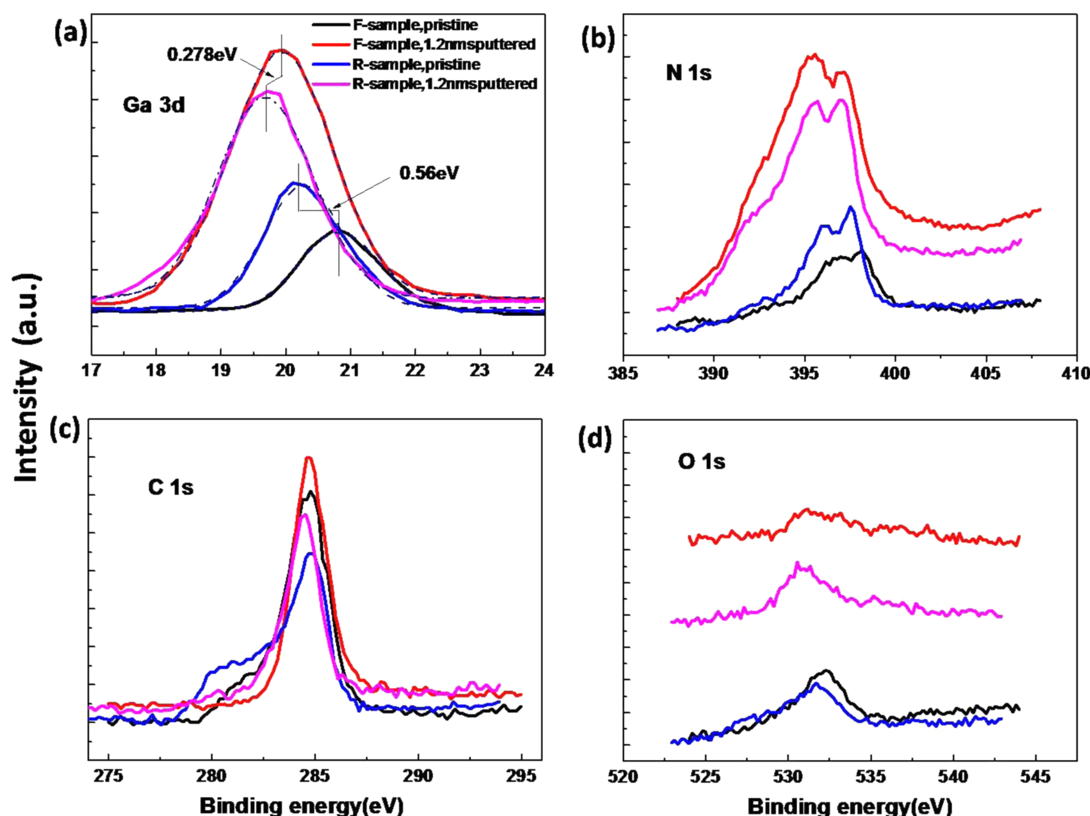

Figure 2. XPS spectral of the (a) Ga 3d, (b) O1s, (c) C 1s, and (d) N 1s core levels for pristine and 1.2 nm sputtered F-, R-samples.

2. EXPERIMENTAL SECTION

A conventional GaN-based epitaxial wafer was grown on a (0001) oriented sapphire substrate by the metal organic chemical vapor deposition (MOCVD) process, containing unintentionally doped GaN (u-GaN) layer (2 μm) and n-type GaN:Si layer (2 μm). After the growth procedure, Cu was electroplated as a new substrate. Sapphire substrate was separated from GaN layer by laser lift off (LLO) process using a KrF exciter laser (248 nm). The residual Ga droplets on the exposed N-polar u-GaN layer were removed by HCl solution. Further inductively coupled plasma (ICP) process to n-GaN layer was performed. The R-sample was then wet-etched in 70 °C 2 mol/L KOH etchant for 10 min. Metal contacts consisted of Al (500 nm)/Ti (50 nm)/Au (500 nm) and Ni (50 nm)/Au (500 nm) were then deposited using electron beam method (EB) at room temperature ambience and elevated vacuum (3.0×10^{-6} Torr). *I*−*V* curves were obtained from model LED-632HC LED Tester (Wei Min Industrial Co., Ltd.). X-ray photoemission spectroscopy (XPS) was employed to investigate the sample surfaces.

3. RESULTS AND DISCUSSION

3.1. *I*−*V* Test. Figure 1a shows the *I*−*V* curves of Al/Ti/Au contacts to F-sample and R-sample. It is shown that Al/Ti/Au could form ohmic contacts to both F-sample and R-sample, which can be indicated from the linear characteristics of *I*−*V* curves. This is due to the comparable work functions of Al (∼4.0−4.2 eV) to n-GaN (∼4.1 eV) and high probability of electron tunneling component.[8] However, R-sample exhibits higher contact resistivity than F-sample. A circular transmission line method (CTLM) pattern with uniform interface area was then used, from which R_c values were calculated to be $\sim 2.5 \times 10^{-5}$ Ω cm^2 and $\sim 1.3 \times 10^{-6}$ Ω cm^2 for R- and F-sample, respectively.

Ni/Au contact to F-sample also shows increased current compared with that of R-sample, as shown in Figure 1b. Different from Al/Ti/Au contacts, an obvious rectifying behavior was observed in Ni/Au contacts to both sample,

dx.doi.org/10.1021/am401354z | ACS Appl. Mater. Interfaces 2013, 5, 5797−5803

due to the work function mismatch between Ni (~5.04−5.35 eV) and n-GaN (~4.1 eV). Based on the work function of Ni and n-GaN, the barrier height Ψ_b could theoretically obtained to be ~1.1 eV (We denote theoretically obtained Ψ_b to be Ψ_b^T). Effective barrier height Ψ_b can be experimentally obtained by the least-squares method using the following equation[10]

$$I = AA^*T^2\exp(-q\psi_b/kT)[\exp(qV/nkT) - 1] \quad (1)$$

Where A is the contact area, A^* is the Richardson constant (26.4 A cm^{-2} K^{-2} for n-GaN), and n is the ideality factor. Taking Ψ_b and n as fitting parameters, Ψ_b can be statistically fitted to be ~0.154 eV and ~0.386 eV for Ni/Au contacts to F- and R-sample (We denote the fitted Ψ_b to be Ψ_b^F), respectively, which is much lower than Ψ_b^T. The discrepancy between Ψ_b^F and Ψ_b^T could be attributed to the large fraction tunneling carrier transportation component (I_T),[9−12] whose flow path is in parallel with the thermal emission-diffusion component ($I_{TD,E}$). So the tested current above (I in eq 1) is actually the sum of I_T and $I_{TD,E}$, hence Ψ_b^F (~0.154 eV and ~0.386 eV) is actually counterfeit barrier height. This has been explicitly illustrated in our earlier reports.[12] Nevertheless, based on Ψ_b^F and Ψ_b^T values, we can roughly estimate the fraction of the I_T component and have a relatively comparison between the carriers interface transport properties of F- and R-sample. The huge discrepancy between Ψ_b^F (~0.154 eV and ~0.386 eV) and Ψ_b^T (1.1 eV) convinces us that tunneling mechanism actually dominates the carrier transportation process in metal/GaN contact.

3.2. Surface-State Investigation by XPS. Differences of contact electrical characteristics between F-, R-sample might be caused by different surface states. To investigate the surface state, were performed XPS measurements, and calibrated the binding energy with C1s = 284.8 eV. As defects generated by LLO are usually within tens of nanometers in depth,[13] for thorough investigation, we also chose to perform XPS measurement after 1.2 nm depth local sputtering. A deeper sputtering will inevitably cause crystal damage and distract to reveal the real interface property. Figure 2 shows XPS spectral of the (a) Ga 3d, (b) O1s, (c) C 1s, and (d) N 1s core levels for pristine and sputtered F-, R-samples. To investigate each bond of Ga−N and Ga−O, we deconvoluted the Ga 3d peaks with Gaussian function, in which Ga−N and Ga−O peaks were assumed to have an energy separation of 0.9 eV (not shown). It is obviously noted that, compared to that of the F-sample, Ga 3d peak of R-sample is slightly shifted toward the lower binding energy side by 0.278 eV and 0.56 eV shift for pristine and sputtered samples, respectively. R-sample peaks of N 1s(b) and O1s(d) also red shift with the same trend. Peaks of C1s keep constant, based on which our XPS measurements are calibrated. XPS peak energy is correspondent to E_F−E_{cl}(i), as denoted in Figure 3a, and E_{cl}(i) represents the intrinsic n-GaN body energy level. Red-shift of XPS peak energy indicates the down shift of Fermi energy level (E_F) of the R-sample, leading to lower electron concentration (N_e). Figure 3a sketches the band diagram for metallization contact to F- (black line), R-sample (red line). As tunneling dominates the I−V characteristics, lowering of N_e in R-sample will obviously widen the space charge layer and bring up the Ψ_b, results to higher R_c, which is in agreement with the former obtained I−V characteristics shown in panels a and b in Figure 1. The increased SBH is also attributed to increased E_c−E_F (Ψ_b = E_C−E_F + V_D).

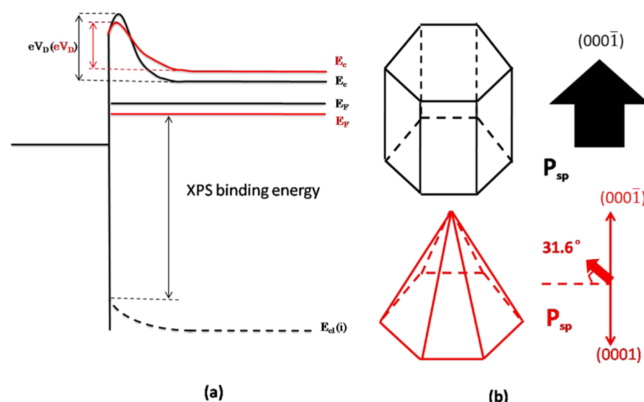

Figure 3. (a) Schematic band diagram on surface band bending for F-sample (black line) and R-sample (red line); (b) schematic drawings of the spontaneous polarization in F-sample (up) and R-sample (bottom). Arrows represent the direction and relative magnitude of spontaneous polarization.

In the following, we will discuss the reason account for electron concentration reduction in R-sample. Apart from the intrinsic material defects and impurities introduced during the epitaxial material growth in MOCVD (as N vacancy (V_N), impurity O and C), various defects and surface states could be generated during LLO and ICP process, as have confirmed by many reports.[14,15] Behave as donors (as impurity O, V_N) or acceptors (as C impurity), these defects and impurities have a significant influence on electron concentration and thus electrical properties. For the R-sample, the wet-etching process would change the surface morphology and surface state, dissolved the encountering defects, impurities and exposed the new orientation surface. We assume the surface state variation as a major reason accounting for the electrical discrepancy between R- and F-sample. First we investigate XPS results for pristine F- and R-sample (black, blue line in Figure 2a−d). For R-sample compared with F-sample, the intensities of Ga 3d, N 1s were increased, C 1s intensity decreased, and O 1s remains almost constant, indicating the etching away of V_N and C, increased Ga−N bond percentage (correspondents to less N vacancy), and decreased C impurity in R-sample. N vacancy and C atom behave as donorlike and acceptorlike impurities in GaN, and electrical compensation may occurs, resulting in electron concentration reduction and so an increase of the effective SBH in R-sample. Then let us investigate the XPS results for 1.2 nm sputtered F-, R-sample (red, pink line in Figure 2a−d. For R-sample compared with F-sample, the intensities of Ga 3d, N 1s, C 1s, and O1s were all decreased, indicating decreased Ga−N bond percentage and decreased C and O impurities in R-sample. We assume the O reduction accounts for the major reason for electron concentration reduction in R-sample. Overall, the precise mechanism responsible for the discrepancy between F- and R-sample are still not certain, because of the existence of multidefects and impurities and the complicated transformation among them, i.e., V_N + O → O_N and V_{Ga} + O_N → V_{Ga}−O_N. What should be noted is that the Ga 3d binding energy shift of R-sample decreased after 1.2 nm sputtered, from 0.56 to 0.278 eV, as shown in Figure 2a. This implies that the defects locate mostly on the surface within depth of several nanometers, and that the Fermi energy levels far away from the surface would be equal to each other, because of the same n-GaN layers being used for F- and R-samples.

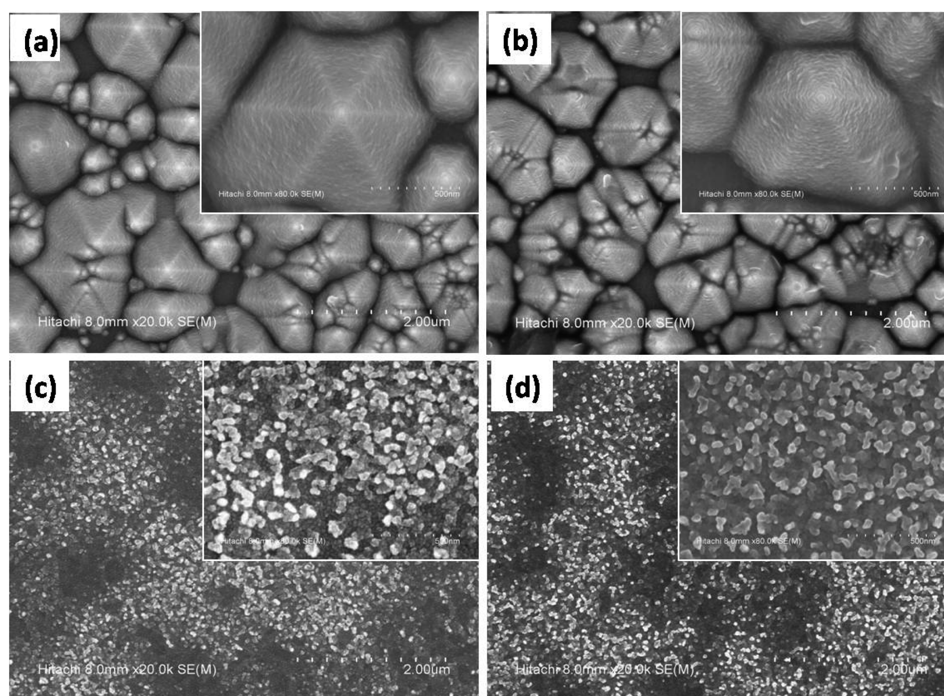

Figure 4. SEM images of metal Al: (a) 0.1 Å/s, R-sample; (b) 10 Å/s, R-sample; (c) 0.1 Å/s, F-sample; (d) 10 Å/s, F-sample.

3.3. Effects of Spontaneous Polarization. Jang and Karrer[16,17] have compared the band bending of metal Pt contacts to Ga-polar and N-polar n-GaN, and found that the SBH for Ga-polar (1.2 eV) was higher than that of N-polar sample (0.9 eV), which was explained by spontaneous polarization discrepancy. Kim[18] also found SBHs of nonpolar a-plane n-GaN was smaller than that of Ga-polar sample by 0.33 eV. Rizzi and Lüth et al.[19] have investigated the SBHs of Ga-and N-polar n-GaN, the result shows that the difference of SBH could be explained in terms of the polarization-induced surface charges in accordance with metal-induced gap state (MIGS) model. These analyses can also be applied to our work. The direction of the spontaneous polarization (P_{sp}) in F-sample is built from the bulk to the surface (Figure 3b, up). Consequently, the negatively bound charges were induced at the surface of the F-sample by spontaneous polarization, leading to the lower upward surface band bending. Different from the F-sample, in the R-sample, the contact metal was actually mostly deposited on semipolar plane with angle of ~58.4° to the $(000\overline{1})$ face, corresponding to $(11\overline{2}\overline{2})$ plane, as can be seen from the SEM image (see the Supporting Information , Figures 1c andd 3c, bottom). It should be noted that the surface polarity of inclined $(11\overline{2}\overline{2})$ planes is not obvious, because it can be terminated by either cations or anions, according only to the crystal symmetry $[20\overline{2}2]$. Considering a tetrahedron crystal structure, the $(11\overline{2}\overline{2})$ plane has been calculated to be N-polar flavor by 20% of the polar $(000\overline{1})$ plane, according to the vector sum of electrical polarization of the four tetrahedral bonds.[20−22] On the basis of these discussions, we concluded that different ratio of spontaneous polarization also contributes to the relatively larger band bending and barrier heights of R-sample, as drawn in Figure 3a.

3.4. Metallization States. In our experiment, the metal atoms were sputtered from crucible by electron beam at room temperature ambience and elevated vacuum, and then migrated for some distance along the receiving substrate surface. Because of the distinct surface roughness of F-, R-sample, we assume that it may lead to different metal state, hence may exert some effect on metal/GaN contact and interface properties. For investigation completeness and prudence, experiment has been carried out. Metal depositing temperature and rate were tentatively considered to influence the metal state. However, high temperature will cause interdiffusion of Ga and metal atoms, which exert an effect on the contact property and thus behave as a distraction. We choose to deposit metal Al (20 nm) at R-sample and F-sample with different depositing rate (0.1 Å/s, 10 Å/s), keeping other deposition parameter (as depositing temperature and pressure) the same. Figure 4 shows the SEM images of metal Al: (a) 0.1 Å/s, R-sample; (b) 10 Å/s, R-sample; (c) 0.1 Å/s, F-sample; (d) 10 Å/s, F-sample. It is shown that Al atoms conforms seamlessly and nearly perfectly to the underlying relief structure in R-sample, with very fine grain size, cannot even be observed on this SEM image. In contrast, Al atoms aggregate on F-sample, with grain size in 50−200 nm range, shows degradation in surface morphology. This discrepancy can be explained in terms of longer migration length, equivalent to stronger ability of Al atoms on F-sample, more likely to overcome the potential barrier and aggregate into large cluster to lower down the total surface energy. Figure 5 shows the $I-V$ curve of the sample, corresponding to Figure 4a−d. There is little discrepancy between curves a and b−d, respectively. This indicates that the effect of different metal states on the contact property between F- and R-sample can be negligible. Because of the great large density of states (DOS), the metal Fermi level could hardly be shifted. The decreased contact resistance for F-sample compared with R-sample at a fixed metal depositing rate (a vs c, b vs d) further confirmed the results shown in Figure 1a.

3.5. Metallization Contact Area. What is more, the area of metallization contact to F- and R-samples should be considered. As can be seen from the Supporting Information,

dx.doi.org/10.1021/am401354z | ACS Appl. Mater. Interfaces 2013, 5, 5797−5803

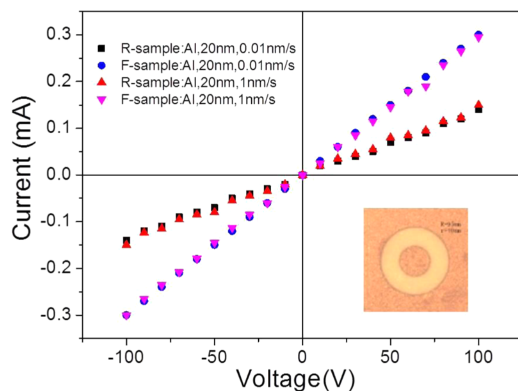

Figure 5. I−V curve of Al (20 nm) to F-, and R-sample, corresponding to Figure 4 a−d, respectively.

Figures 1c, 4a, and 4b, hexagonal pyramids are randomly and densely distributed on the R-sample surface, with a filling factor approaching 100%. So the area of metallization contact to R-sample is about twice of that of the F-sample $[(A_{\text{R-sample}}/A_{\text{F-sample}} \approx 1/\cos(58.4°) \approx 1.9)]$. Keep other parameters invariant, an increased metallization contact area of course brings down the total contact resistivity ($R_c = \rho/S$) and the Ψ_b^F value (eq 1). However, it can be inferred from Figure 1a and Figure 5 that the R_c value of the R-sample is higher than that of the F-sample. Alsom we have shown that the obtained Ψ_b^F value of R-sample is higher than that of F-sample. This contradiction proves the existence of some other factors that would obviously increase the R_c and Ψ_b^F values in the R-sample, counteracting the effect of larger metallization contact area for R-sample.

We further list the multiple factors (surface state, spontaneous polarization, metal deposited state, and metallization contact area) in Table 1, with the purpose to clearly summarize their effect on R_c and Ψ_b^F values of F- and R-sample. As shown in Table 1 and according to discussions above, surface state variation after the wet-etching process and spontaneous polarization discrepancy will bring up R_c and Ψ_b^F values for R-samples, compared with that of F-samples. Instead, a larger metallization contact area will decrease R_c and Ψ_b^F values for R-samples, and the effect of metal deposited state is negligible. The experimental results are the sum up of the multiple effects, the ultimate increase in R_c and Ψ_b^F values for R-samples indicates the dominate effects of surface state and spontaneous polarization. However, we cannot precisely extract the two effects separately, and we just presumably think the surface state variation results from wet-etching is the main reason accounting for the increased R_c and Ψ_b^F values for R-samples.

3.6. Thermal Annealing of Metallization Contacts.

Thermal behavior of metallization contacts to both samples was further investigated by annealing in 250 °CN_2 atmosphere for different time. Panels a and b in Figure 6 show the I−V behavior of Au/Ti/Al contacts to the F- and R-sample, respectively. It is shown that both exhibit degraded I−V behaviors upon annealing. R_c values were calculated to be about 7.5×10^{-6} Ω cm^2 (1 min), 4.2×10^{-5} Ω cm^2 (2 min), and 6.1×10^{-5} Ω cm^2 (3 min) for the F-sample and 3.9×10^{-5} Ω cm^2 (1 min), 5.2×10^{-5} Ω cm^2 (2 min), and 7.1×10^{-5} Ω cm^2 (3 min) for the R-sample, respectively. Different with Ga-polar GaN or mostly other metallization/semiconductor contact, N-polar GaN/metal contact unambiguously degraded after thermal annealing, as reported and concluded by our group and any other group.[4,5,8,18] Reason accounting for this have been widely investigated and discussed.[4,5,23] We think surface state variation during annealing process is the mainly contribute to its degradation. However, it is clear that the degradation of the contact on F-sample is faster than that on R-sample. At the end of the annealing process, contact resistances on both sample become similar. It cannot be simply explained by the formation of interfacial AlN, which increases the effective SBH because of the opposite spontaneous polarization field of the N-polar GaN.[24] From XPS comparison of bare N-polar n-GaN, Hyunsoo has found that the Ga3d peak was shifted toward the lower binding energy side after annealing,[4] which indicates a downshift of the Fermi level energy and a decrease in the electron concentration due to loss of V_N upon annealing. This analysis is consistent with our experiment. As the V_N density in the F-sample is relatively higher than in the R-sample before annealing, the annealing process will cause a loss of V_N, and this is more obvious in the F-sample, leading to more severe degradation of I−V behavior. It should be noted that the degradation becomes less significant in both samples with increased annealing time, this indicates equilibrium state of V_N approaches for both. I−V behavior of Au/Ni contacts to F-, R-sample shows the similar degradation upon annealing for different time, as shown in Figure 6c. Also by introducing eq 1, Ψ_b^F were fitted to be ∼0.184 eV(1 min), ∼0.325 eV (2 min), ∼0.351 eV(3 min) for F-sample, and ∼0.392 eV(1 min), ∼0.59 eV(2 min), ∼0.68 eV(3 min) for the R-sample, respectively. Annealing process is helpful for crystalline imperfections recovery, leading to decrease of impurity O and C, V_N. This will bring down the probability for electron tunneling across the metal−GaN interface, thus increasing the Ψ_b^F value.

3.7. Vertical Light-Emitting Diode Fabrication.

On the basis of the analysis above, two sets of VLEDs were fabricated with n-contact metal deposited on Flat (F-VLEDs) and wet-etching roughed (R-VLEDs) N-polar GaN, respectively. The detailed fabrication process is similar as in a previous report[25]

Table 1. Summary of the Effect of Each Factor on R_c and Ψ_b^F Values of R-sample, Compared with That of F-Sample

	Surface state	Spontaneous polarization	Metal state	Metallization contact area	Experimental results
Rc, Ψ_b^Fvalues variation (R-sample)	↑	↑	—	↓	↑

dx.doi.org/10.1021/am401354z | ACS Appl. Mater. Interfaces 2013, 5, 5797−5803

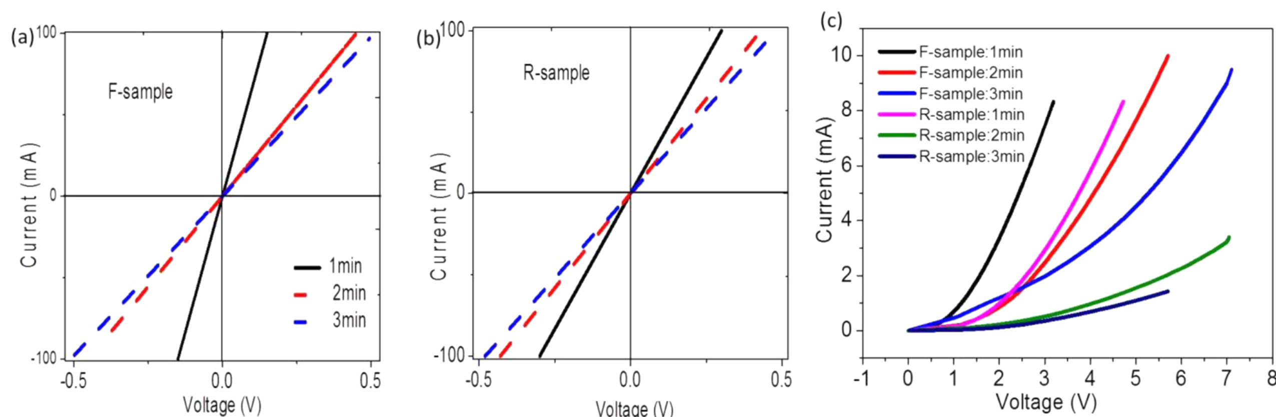

Figure 6. $I-V$ curves of Al/Ti/Au contacts to (a) F-sample and (b) R-sample after annealing in 250 °C N_2 atmosphere for different times; (c) $I-V$ behavior of Au/Ni contacts to F-, R-sample upon annealing for different times.

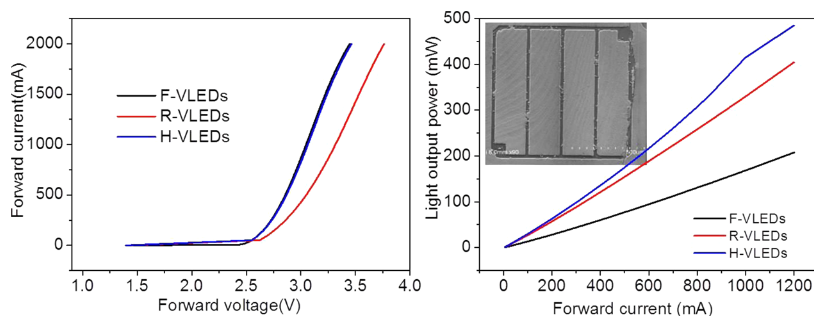

Figure 7. (a) Electrical and (b) optical characteristics of F-VLEDs, R-VLEDs, and H-VLEDs.

(see the Supporting Information, Figure 1a). After being diced into a 1 mm × 1 mm chip, VLEDs chips were packaged and tested. The typical $I-V$ curves were plotted in Figure 7a, F-VLEDs shows extremely low forward voltage (V_F) (2.75 V@ 350 mA, 3.04 V@1000 mA, and 3.44 V@2000 mA), lower than that of R-VLEDs (2.94 V@350 mA, 3.32 V@1000 mA, and 3.76 V@ 2000 mA). This is also among the lowest V_F value reported for LEDs with the comparable size (usually 45 × 45 mil for L-LEDs and 1 mm × 1 mm for VLEDs).The increased V_F of R-VLEDs is attributed to the increased metal/N-polar n-GaN R_c value. These VLED chip results further confirmed our comparison analysis between the F- and R-sample above. However, as we all know, wet-etching roughing process is a common and necessary way to increase the light output of VLEDs. Compared with R-VLEDs, the light output power (LOP) of F-VLEDs undoubtedly decreased, about half of the LOP of R-VLEDs, as shown in Figure 7b. We have successfully developed a hybrid scheme of F- and R-VLEDs through a selective wet -etching approach, that is, only the nonmetal pattern area was wet-etched and the contact metal was deposited on flat N-polar GaN surface, as can be figured from the SEM image shown in the inset of Figure 7b. The hybrid scheme will retain the advantages of both F- and R-samples, optimized to bring down the V_F and increase the LOP simultaneously. The Supporting Information, Figure 2, sketches the structure of F-VLEDs, R-VLEDs, and H-VLEDs. Figure 7a also shows the $I-V$ behavior of hybrid scheme-based VLEDs (H-VLEDs), which is almost overlap with F-VLEDs, much lower than that of R-VLEDs. Figure 7b shows the LOP characteristics of F-, R- and H-VLEDs. LOP of H-VLEDs was substantially increased by 140% and 40% compared with that of F-VLEDs and R-VLEDs, respectively. This is attributed to the selectively wet-etching roughing and the reduced power dissipation with improved electrical characteristics.

CONCLUSION

To conclude, the electrical characteristics of metal contacts to F-sample and R-sample have been investigated. R-sample shows higher R_c (2.5×10^{-5} Ω cm^2) and higher SBH (0.386 eV), compared that of F-sample (1.3×10^{-6} Ω cm^2, 0.154 eV). Reasons accounting for this discrepancy has been discussed: (i) the wet-etching process dissolves the encountering defects (as V_N), impurities (as atom O and C), an electrical compensation results to a decrease in the electron concentration in the R-sample, as revealed by XPS results; (ii) metal was deposited on the semipolar $(11\overline{2}\overline{2})$ plane in the R-sample and the $(000\overline{1})$ plane in the F-sample, and different ratios of spontaneous polarization also contribute to the relatively larger band bending and SBH in the R-sample; (iii) the deposited metal is smoother in the R-sample than in the F-sample, yet the effect of different metal state on the contact and interface property between F- and R-sample can be negligible. $I-V$ behaviors after annealing have also been investigated, and R-sample shows alleviated degradation than F-sample. We believe this understanding of the contact to N-polar n-GaN is crucial to the development of noble metallization contacts for the VLEDs, chip $I-V$ results further convinced our analysis.

ASSOCIATED CONTENT

Supporting Information

Supporting Figure 1a presents the fabrication process of F-sample and R-sample. The fabrication process of F-sample is similar with the conventional vertical light-emitting diodes, including: mirror metal and copper substrate electroplating,

laser lift off process to detach sapphire. The R-sample is obtained by dipping the F-sample in 70 °C KOH solution for ~10 min. Images b and c in Supporting Figure 1 show the SEM images of F-sample and R-sample surface, respectively. Supporting Figure 2 sketches the chip structure of the F-VLEDs, R-VLEDs, and H-VLEDs. This material is available free of charge via the Internet at http://pubs.acs.org.

■ AUTHOR INFORMATION

Corresponding Author

*E-mail: wanglc@semi.ac.cn (L.W.); spring@semi.ac.cn (X.Y.). Tel: (+86)10-82305458.

Notes

The authors declare no competing financial interest.

■ ACKNOWLEDGMENTS

This work was supported by the National High Technology Program of China (2011AA03A105 and 2013AA03A101), National Natural Science Foundation of China (60806001 and 50972067), and National Basic Research Program of China (2011CB301904 and 2011CB013000).

■ REFERENCES

(1) Liu, Z.; Wei, T.; Guo, E.; Yi, X.; Wang, L.; Wang, J.; Wang, G.; Shi, Y.; Ferguson, L.; Li, J. *Appl. Phys. Lett.* **2011**, *99*, 091104.

(2) Hibbard, D. L.; Jung, S. P.; Wang, C.; Ullery, D.; Zhao, Y. S.; Lee, H. P.; So, W.; Liu, H. *Appl. Phys. Lett.* **2003**, *83* (2), 311.

(3) Tan, B. S.; Yuan, S.; Kang, X. J. *Appl. Phys. Lett.* **2004**, *84* (15), 2757.

(4) Kim, H.; Ryou, J.-H.; Dupuis, R. D.; Lee, S.-N.; Park, Y.; Jeon, J.-W.; Seong, T.-Y. *Appl. Phys. Lett.* **2008**, *93* (19), 192106.

(5) Jang, H. W.; Lee, J.-L. *Appl. Phys. Lett.* **2009**, *94* (18), 182108.

(6) Fujii, T.; Gao, Y.; Sharma, R.; Hu, E. L.; DenBaars, S. P.; Nakamura, S. *Appl. Phys. Lett.* **2004**, *84* (6), 855.

(7) Qi, S. L.; Chen, Z. Z.; Fang, H.; Sun, Y. J.; Sang, L. W.; Yang, X. L.; Zhao, L. B.; Tian, P. F.; Deng, J. J.; Tao, Y. B.; Yu, T. J.; Qin, Z. X.; Zhang, G. Y. *Appl. Phys. Lett.* **2009**, *95* (7), 071114.

(8) Wang, L.; Guo, E.; Liu, Z.; Yi, X.; Wang, G. *SOPO* **2011**, DOI: 10.1109/SOPO.2011.5780596..

(9) Yu, L. S.; Liu, Q. Z.; Xing, Q. J.; Qiao, D. J.; Lau, S. S.; Redwing, J. *J. Appl. Phys.* **1998**, *84* (4), 2099.

(10) Sze, S. M.; and Ng, K. K. In *Physics of Semiconductor Devices*, 3rd ed.; Wiley: Hoboken, NJ, 2007.

(11) Yan, D.-W.; Zhu, Z.-M.; Cheng, J.-M.; Gu, X.-F.; Lu, H. *Chin. Phys. Lett.* **2012**, *29* (8), 087204.

(12) Wang, L.; Zhang, Y.; Li, X.; Guo, E.; Liu, Z.; Yi, X.; Zhu, H.; Wang, G. *RSC Advances* **2013**, *3* (10), 3359.

(13) Chen, W. H.; Kang, X. N.; Hu, X. D.; Lee, R.; Wang, Y. J.; Yu, T. J.; Yang, Z. J.; Zhang, G. Y.; Shan, L.; Liu, K. X.; Shan, X. D.; You, L. P.; Yu, D. P. *Appl. Phys. Lett.* **2007**, *91* (12), 121114.

(14) Picozzi, S.; Continenza, A.; Satta, G.; Massidda, S.; Freeman, A. J. *Phys. Rev. B* **2000**, *61*, 16736.

(15) Cho, H. K.; Kim, S.-K.; Lee, J. S. *J. Phys. D: Appl. Phys.* **2008**, *41* (17), 175107.

(16) Jang, H. W.; Lee, J.-H.; Lee, J.-L. *Appl. Phys. Lett.* **2002**, *80* (21), 3955.

(17) Karrer, U.; Ambacher, O.; Stutzmann, M. *Appl. Phys. Lett.* **2000**, *77* (13), 2012.

(18) Kim, H.; Lee, S.-N.; Park, Y.; Kwak, J. S.; Seong, T.-Y. *Appl. Phys. Lett.* **2008**, *93* (3), 032105.

(19) Rizzi, A.; Lüth, H. *Appl. Phys. Lett.* **2002**, *80* (3), 530.

(20) Masui, H.; Cruz, S. C.; Nakamura, S.; DenBaars, S. P. *J. Electron. Mater.* **2009**, *38* (6), 756–760.

(21) Masui, H.; DenBaars, S. P.; Mishra, U. K. *IEEE Trans. Electron. Dev.* **2010**, *57* (1), 88.

(22) Bernardini, F.; Fiorentini, V.; Vanderbilt, D. *Phys. Rev. B* **1997**, *56*, 10024.

(23) Kim, J. K.; Jang, H. W.; Kim, C. C.; Je, J. H.; Rickert, K. A.; Kuech, T. F.; Lee, J.-L. *J. Vac. Sci. Technol. B* **2003**, *21* (1), 87.

(24) Luther, B. P.; DeLucca, J. M.; Mohney, S. E.; Karlicek, R. F. *Appl. Phys. Lett.* **1997**, *71*, 3859.

(25) Wang, L.; Zhang, Y.; Li, X.; Liu, Z.; Guo, E.; Yi, X.; Wang, J.; Zhu, H.; Wang, G. *Appl. Phys. Lett.* **2012**, *101* (6), 061102.